Open Ceramics 19 (2024) 100659

Contents lists available at ScienceDirect

Open Ceramics

journal homepage: www.sciencedirect.com/journal/open-ceramics

Reused green glass for the production of low-density ceramic proppants

Ricardo Anaya [a,b,*], María F. Hernández [a,b], Anabella Mocciaro [a], Diego Richard [a,b], Nicolás M. Rendtorff [a,b]

[a] CETMIC, Centro de Tecnología de Recursos Minerales y Cerámica (CONICET La Plata - CIC PBA - UNLP), Cno. Centenario y 506, 1987, M. B. Gonnet, Buenos Aires, Argentina
[b] Facultad de Ciencias Exactas, Universidad Nacional de La Plata, Calle 1 y 47, 1900, La Plata, Buenos Aires, Argentina

ARTICLE INFO

Handling Editor: Dr P Colombo

Keywords:
Ceramic low-density proppants
Circular economy
Waste glass
Processing and properties

ABSTRACT

The reuse of waste to promote manufacturing processes that are respectful of the environment is a fundamental requirement in circular economy practices. In this work, it is assessed the feasibility of manufacturing ceramic proppants from a commercial red clay, sodium and potassium feldspars, and significant amounts of green bottle glass recovered from urban wastes.

Different ceramic mixtures were formulated, and the sintering conditions were defined considering optical dilatometric, differential thermal, and thermogravimetric analysis. The obtained granules were characterised following the international standard for proppants, and also using X-ray diffraction, scanning electron microscopy, and individual diametral compression tests.

The results show that competitive proppants are obtained, due to their low-density (2.5 g/cm^3) and good breakage ratio (7.8 % at 5000 psi, or 34.5 MPa), but also considering the involved low-cost processing route and raw materials.

1. Introduction

Hydraulic fracturing is a method widely used for the extraction of oil and gas in unconventional reservoirs. A fracturing fluid (generally water with different additives) is injected at high pressures, to produce cracks in the rock through which the hydrocarbons will flow. These cracks are kept open using a particulate material, called proppant, that acts as support forming a porous package and maintaining its permeability during the production of the well. An ideal proppant must have adequate chemical and mechanical resistance, and promote adequate permeability to allow the extraction of hydrocarbons efficiently [1]. The main materials used to produce proppants are quartz sand or silica-alumina ceramics. Ceramic proppants have a high cost but are widely used because of their mechanical resistance and permeability [2,3].

One possible proppant classification is according to its apparent density. Low, intermediate, and high-density proppants can be defined with ranges from 2.5 to 3.9 g/cm^3 [4]. The mechanical resistance of proppants generally has a direct relationship with their density and alumina content [3]. A higher alumina content significantly increases the strength of the proppants as well as their density. However, their production cost also increases due to the high temperatures necessary for sintering [5], and the cost during their use also increases because high-density proppants require more expensive pumping proppants-fracturing fluids [1]. Therefore, the development of lightweight ceramic proppants is a challenge that can help to overcome some of these processing disadvantages [4,6,7]. Now the world has been focused on pursuing meaningful action to reduce resources and environmental pressures, the strategic use of waste as raw material in the industrial processes is one of the solutions that are proposed in the circular economy model [8,9]. Red ceramics are a very promising candidates for this purpose due to their versatility in terms of the wide variety of raw materials that can be used. The waste incorporation in a ceramic formulation can modify its plasticity, its density after fired (flux agents), its shrinkage during firing (filler), among other properties. However, there is still a lack of studies that address the incorporation of recycled waste and its relationship with the manufacturing process and the technological behaviour of the ceramic products [8]. Furthermore, it is well known that the demand for proppants in hydraulic fracturing operations is significant and that there are currently no tailings available in

* Corresponding author. CETMIC, Centro de Tecnología de Recursos Minerales y Cerámica (CONICET La Plata - CIC PBA - UNLP), Cno. Centenario y 506, 1987, M. B. Gonnet, Buenos Aires, Argentina.
E-mail address: ricardoanaya@cetmic.unlp.edu.ar (R. Anaya).

https://doi.org/10.1016/j.oceram.2024.100659
Received 24 May 2024; Received in revised form 9 August 2024; Accepted 13 August 2024
Available online 16 August 2024

sufficient quantities to replace traditional proppants. In this regard, recent research has been conducted on the development of proppants that include industrial wastes from different sources. Some studies evaluated the incorporation of fly ash as a raw material to produce low-density proppants from fly ash and bauxite [2,10], while other studies combined fly ash with drilling coats [11], and with red mud from Bayer process [12] in the proppant formulation. Another attractive alternative for the production of proppant ceramics is the use of waste glass as raw material.

Glass recycling has environmental benefits related to the conservation of natural resources and the reduction of pressure on landfills, as well as energy savings and cost reductions due to the presence of flux agents in its composition. Depending on the manufacturing process, end use and materials incorporated, the resulting glass-ceramic can exhibit high mechanical performance with zero porosity or an extremely porous material with excellent insulating properties, among other positive characteristics [13–16]. The temperature and time of sintering of the materials must also be taken into account, since increasing the glass content can improve the degree of crystallisation and densification, resulting in better mechanical performance at lower temperatures [8, 17].

The main objective of this work is to evaluate the applicability of waste glass as raw material for the manufacture of low-density ceramic proppants and to describe the ceramic behaviour of formulations with up to 40 wt% of this raw material in terms of the formulation-processing-properties relations. Furthermore, it is intended to describe the thermal behaviour, sintering, and technological properties of the resulting materials, depending on the firing temperature and the proportion of glass. Considering all the above, the proppants elaborated at lab-scale were evaluated by means of American Petroleum Institute (API) 19C standard. These characterizations consist of crush resistance test, bulk density, apparent density and acid solubility.

Finally, the results of this systematic study with bottle glass in proppant formulation may be extrapolated to other industrial or urban glass wastes, with similar chemical composition and properties. Therefore, this work may also contribute to the understanding of proppants formulation strategies with sustainable criteria.

2. Material and methods

2.1. Raw materials

An industrial kaolinitic clay (APM, Piedra Grande - La Toma; Neuquén, Argentina) was used as a source of Al_2O_3 and SiO_2 and to give certain plasticity to the mixtures [18,19], sodium and potassium feldspar ($NaAlSiO_8$ and $KAlSiO_8$; Piedra Grande, Argentina) was used as a flux [10]. Green glass from recycled wine bottles was also employed as a secondary source of SiO_2 and complementary fluxing agent. Table 1 shows the chemical composition of the raw materials used in this study, in the case of green glass the composition was estimated according to literature [20].

2.2. Starting mixture processing

APM clay and feldspar are commercialised under a grain size below 0.074 mm (mesh #200). The green glass was dry ground in a ball mill to a powder with the same grain size as the other raw materials. To this purpose a porcelain jar and alumina balls were used in a glass:ball volume ratio 1:1. A part of the APM clay was calcined at 700 °C during 30 min to reduce plasticity in the mixtures, because a high plasticity does not allow correct granulation.

Four mixtures were formulated and their compositions are listed in Table 2. A different proportion of green glass was added in each mixture: 0, 10, 20, and 40 wt%, which are labelled G0, G10, G20, and G40, respectively. In all the mixtures 20 wt% of un-calcined clay and 10 wt% of feldspar were incorporated, so the proportion of calcined clay gradually decreases with the increase of glass content. Table 3 shows the chemical composition of the mixtures theoretically calculated.

2.3. Proppants granulation

To granulate the mixtures, an intensive mixer, Eirich model R02E with a nominal capacity of 5 L was used [21–23]. The proppant granulation program was tuned to obtain an adequate distribution size according to the application requirements. The rotation speed of the vessel was 45 rpm and the mixing tool rotated at 1900 rpm in the granulation stage during 300 s and at 200 rpm in the granule spherization stage for 300 s. The rotation of the vessel and the mixing tool were in opposite directions. Each batch of material was made with 1 kg of the dried mix and between 150 and 200 mL of tap water as binding liquid.

After the shaped process, the granules were dried at 120 °C for 24 h and then, were sieved through #16 mesh (1.18 mm) in order to eliminate large agglomerates and large grains (which represented less than 5 wt% in all the cases). The resulting granules were sintered at a temperature between 1050 and 1200 °C in an electric furnace in air atmosphere, using a heating rate of 10 °C min^{-1} and 30 min soaking. Two firing temperatures for each mixture were defined after the analysis of the dilatometric curves, choosing different stages of the sintering process as will described below.

2.4. Starting mixtures characterization

Thermal behaviour of the mixtures was studied by thermogravimetric (TG), differential thermal analysis (DTA), and optical dilatometry. The TG-DTA curves allow the study of the chemical behaviour of each powder upon heating [24]. Both curves were simultaneously measured in a Netzsch STA 409c equipment, placing 300 mg of each powder in a platinum crucible and using a constant heating rate of 10 °Cmin^{-1} and a standard alumina reference.

On the other hand, optical dilatometry measurements were performed to study the sample shrinkage, using a Linseis L74 optical dilatometer, air atmosphere and a heating ramp of 10 °C min^{-1} up to 1350 °C [25]. This test was carried out on cylindrical specimens of approximately 4 mm diameter and 5 mm length (L_o), which were prepared by manual pressing (≈2 MPa). The curves of length ratio (L/L_o) versus temperature obtained from these tests were used to determine the temperature of sintering, as will be discussed later.

Table 2
Starting mass composition of the considered mixtures in this study (wt.%).

Mixture	APM clay	Calcined APM clay	Feldspar	Green glass
G0	20	70	10	0
G10	20	60	10	10
G20	20	50	10	20
G40	20	30	10	40

Table 1
Chemical composition of the raw materials.

Raw materials	SiO_2	Al_2O_3	Na_2O	K_2O	CaO	MgO	Fe_2O_3	TiO_2
APM clay	59.5	32.6	0.1	1.5	0.2	0.9	4.2	1.0
Green glass [20]	71.8	2.46	12.74	–	10.21	2.05	0.42	
Feldspar	66.0	18.5	2.5	12.5	0.2	–	–	–

Table 3
Theoretical chemical composition of the considered mixtures.

Mixture	SiO_2	Al_2O_3	Na_2O	K_2O	CaO	MgO	Fe_2O_3	TiO_2
G0	60.2	31.2	0.4	2.5	0.2	0.7	3.7	0.8
G10	61.4	28.2	1.6	2.4	1.2	0.9	3.3	0.8
G20	62.6	25.1	2.9	2.2	2.2	1.0	2.9	0.7
G40	65.1	19.1	5.4	1.9	4.2	1.3	2.1	0.5

2.5. Standard proppant characterization

API 19C standard was used in order to evaluate the final technical properties of the different materials and compare them with the specifications established in this standard [26,27].

The granulometric distribution of the proppants obtained after firing was analysed using mesh sieves #20, #30, #40, #50, and #70, which correspond to aperture sizes 0.840, 0.590, 0.420, 0.297, and 0.210 mm, respectively. Considering that the size range of meshes #20 to #40 is commonly used in hydraulic stimulation operations in unconventional reservoirs [1,28], proppants from this fraction were used to perform the characterization tests.

Sphericity and roundness were determined using Krumbein and Sloss chart. To this purpose, images on an average of twenty particles were taken with a stereoscopic microscope (Leica SAPO) [1].

Bulk and apparent density were determined according to the standard API 19 C. The bulk density evaluates the mass per unit volume, including the space between particles and it is related to the packaging of the granules. A fixed volume is filled with a sample of proppant and then weighed. In contrast, the apparent density evaluates the mass per unit volume of the particles, including their internal porosity, and it and was measured by pycnometry.

The crush resistance test was performed under 5000 Psi (34.5 MPa). The breakage ratio percentage was calculated using the following relation: $100 \times \frac{w_c}{w_o}$, where w_c is the mass of crushed specimens after testing and w_o is the mass of proppants before testing. For this test, the final breakage ratio value was obtained from the average of three measurements [28].

On the other hand, acid solubility tests were also performed. To this purpose, a known mass of proppants was heated at 66 °C during 30 min in an acid solution (12:3 hydrochloric-hydrofluoric acid). Then, the sample was dried and washed, and the percentage weight loss was determined.

2.6. Complementary proppants characterization

The crystalline phases in the proppants were analysed by X-ray diffraction (XRD), using a Bruker D8 Advance diffractometer operated with Cu-Kα radiation (λ = 1.54 Å). The scan was performed in the 2θ range from 3 to 70°, with a step of 0.02° and a time of 0.5 s per step [29]. Additionally, scans were performed in the 2θ range from 15 to 18° with a step of 0.02° and a time of 5 s per step to evaluate the mullite 110 peak more accurately. This peak was chosen for analysis because it does not overlap with any peaks of other phases.

Scanning electron microscopy (SEM) was used in order to describe the topography and the microstructure of the proppants. Surface structure of the granules were observed. In addition, after the acid solubility test the microstructure of the proppants was also observed for a better visualisation of the crystalline structure, because the acid removes the vitreous phase. The SEM images were taken using a Jeol JCM-6000 equipment on samples coated with silver in high vacuum conditions and with an accelerating voltage of 10–15 kV.

The individual compressive strength was measured to know the mechanical behaviour of the material and estimate the direct pressure that each individual propant can withstand [30]. This test was carried out using a universal testing machine (Instron 5985, USA) at a constant strain rate of 0.018 mm min^{-1} with steel plates. Ten (10) granules were tested for each formulation. The Hertz equation [31] as used to determine the tensile stress (σ_T), considering the proppant as a spherical particle: $\sigma_T = \frac{4kL}{\pi D^2}$ where D is the diameter of the granule, L is the applied load, k is a constant related particle satrain response which in this work is considering a value of $k = 1$.

3. Results and discussion

3.1. Thermal behaviour of the mixtures

Fig. 1 shows the differential thermal analysis and thermogravimetric curves. In all samples, the loss of surface water is observed around 100 °C. The small differences for the water loss between proppants at this temperature could be due to slight differences in the drying process.

The DTA curves show an endothermic peak at 525 °C which is accompanied by a mass loss in the TG curves that take place in the range 400 and 600 °C and is related to the dehydroxylation of kaolinite clay [32]. Because the amount of un-calcined clay is the same in all mixtures, the water loss in this temperature range is similar in all cases (≈1.6 %).

Finally, an exothermic peak is observed in the DTA curve around 938 °C. At this temperature, the SiO_4 and AlO_6 groups combine to give the Al–Si spinel phase, precursor of the mullite phase [33,34]. By increasing the glass content in the mixtures, this peak moves to lower temperatures and, furthermore, tends to disappear in the G40 sample. According to the literature, the addition of fluxes in the formulation modifies this peak and this causes a decrease in the amount of mullite formed during sintering [18,35–37]. Although the formation of mullite in the obtained proppants will be verified later by XRD, the Al_2O_3/SiO_2 ratio in the G40 sample could be not enough to form the spinel phase that leads to the mullite crystal growth (see chemical composition in Table 3). In addition, the greater amount of flux agents (Fe_2O_3, K_2O, CaO, Na_2O, MgO) could generate an excess of vitreous phase during firing that may affect the sintering mechanism.

The dilatometric curve and its derivative are shown in Fig. 2. It is

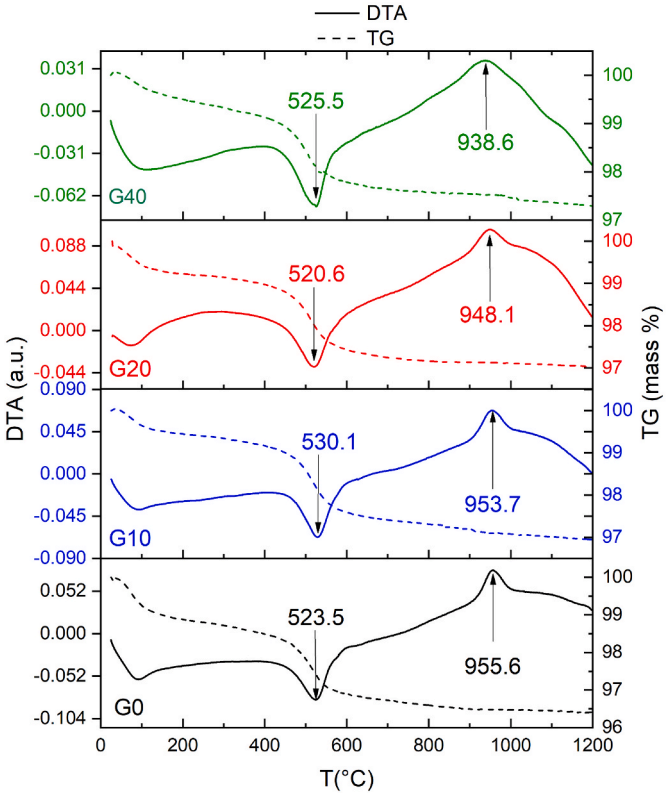

Fig. 1. DTA-TG curves of the different proppant formulation.

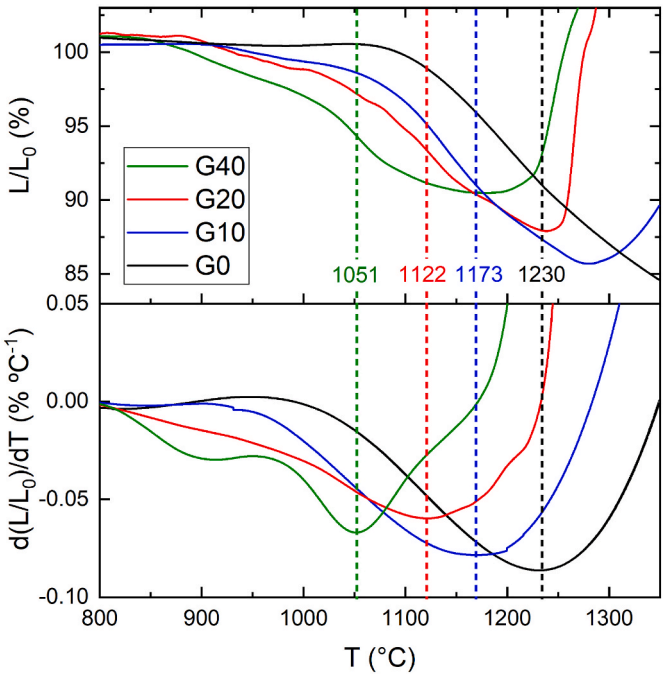

Fig. 2. Dilatometric curves of the mixtures studied (up) and their temperature derivatives (below).

observed that the main dilatometric event happens at temperatures above 900 °C and corresponds to shrinkage of about 10 % or higher. By increasing the amount of green glass in the starting mixtures, the temperature where shrinkage starts shifts towards lower values and the maximum shrinkage decreases and happens at lower temperature. The minima of the derived function indicate the temperature at the inflection point of the dilatometric curves, being 1230, 1173, 1122, and 1051 °C for samples G0, G10, G20, and G40, respectively, as indicated in the graph with the dashed vertical lines [38]. Considering these results, the firing temperatures were chosen in order to achieve different levels of densification of the material. For each mixture, two temperatures were selected: the first value was 1100 °C for all the samples, and the second temperature was 1200 °C for G0 and G10 samples and 1050 °C for G20 and G40 samples. In the following sample naming will contain the proppants formulation and firing temperature.

3.2. Characterization by API 19C standard

Fig. 3 shows the size distribution for the proppants after fired. In general, the size distribution of all the samples are similar, with the most granules between #20/40 mesh, which correspond to sizes in the range 0.420–0.850 mm. Only proppants in this range (highlighted in red) were used in the characterization.

In Fig. 4 stereoscopic microscope images of a representative granules amount of each resulting proppant are presented. Sphericity and roundness values for all the samples are greater than 0.8 and 0.6, respectively. These values are sufficient for the analysis proposed in this work, but can be improved if necessary in future studies by adjusting the processing variables.

The images of Fig. 4 show that, as the green glass content increases, less roughness and greater shine are observed on the granules surface, as a consequence of the greater content of vitreous phases. Sphericity and roundness are related with packaging of the granules in the well. High sphericity and roundness values can improve the conductivity of the hydrocarbons in the fracture [39–41].

Apparent density, bulk density, breakage ratio and acid solubility of the proppants are presented in Table 4. All samples present bulk density values between 1.25 and 1.39 g/cm^3 meanwhile apparent density values

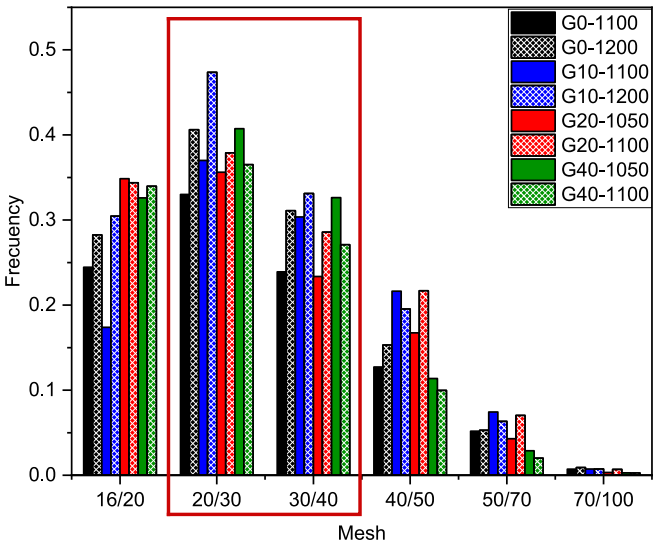

Fig. 3. Size distribution of proppants after fired.

were in the range of 2.43–2.60 g/cm^3; these results classify the resulting materials as low-density proppants.

After firing at 1100 °C as green glass amount in the formulation increases, the apparent density decreases.

Assuming that all proppants have similar crystalline phase according to the chemical composition estimate aforementioned (Table 3) and these phases (quartz, glass and cristobalite) have similar densities, we could consider that the density of the material does not change. Therefore, two main factors affect the apparent density of granules. Firstly, the shrinkage of the material during sintering which is observed in dilatometric curves (Fig. 2), in the range of temperatures evaluated, produces an increase in density. On the other hand, we have the glass content; the increase of green glass amount in the mixture formulation contributes to the decrease of open pores generating an impermeable surface and, as a result, lighter granules. The values of apparent density presented in Table 4 shows that the last effect is the predominant one.

In addition, it is observed that by increasing green glass content and temperature, the bulk density increases slightly. This is related to the shrinkage of the material during sintering.

The standard API 19C requires a breakage ratio less than 10 wt% for the proppant to be used for the hydraulic fracture. According to the values presented in Table 4, G10-1100, G20-1100, and G40-1050 are the only samples that fulfil with this specification.

On the other hand, it is observed that the breakage ratio decreases when the amount of green glass in the formulation increases. For example, G20 has the lowest value when the formulation is fired at 1100 °C, while for G40 the lowest breakage ratio is obtained for 1050 °C. Higher firing temperature or higher flux addition (green glass) to the formulation can improve the sintering process of the material, so that its mechanical strength increases up to a certain point. Beyond this point, the strength resistance of the proppants decreases due to abnormal growth and melting of crystals as well as excess glass phase. Different authors reported comparable values in works where proppants are produced from industrial wastes [10,42,43]. Furthermore, these measurements are similar to those presented by some high-quality fracture sands [44,45].

In relation to acid solubility it is observed that in G0 and G10 fired at 1200 °C presented values lower than 7 wt%, which is in agreement with standard specification. In particular, samples that met the standard requirement for breakage ratio did not meet the established requirements for acid solubility. These last results are associated with the larger amount of green glass in the mixtures (Table 3), which produce a higher vitreous phase in the proppants after fired.

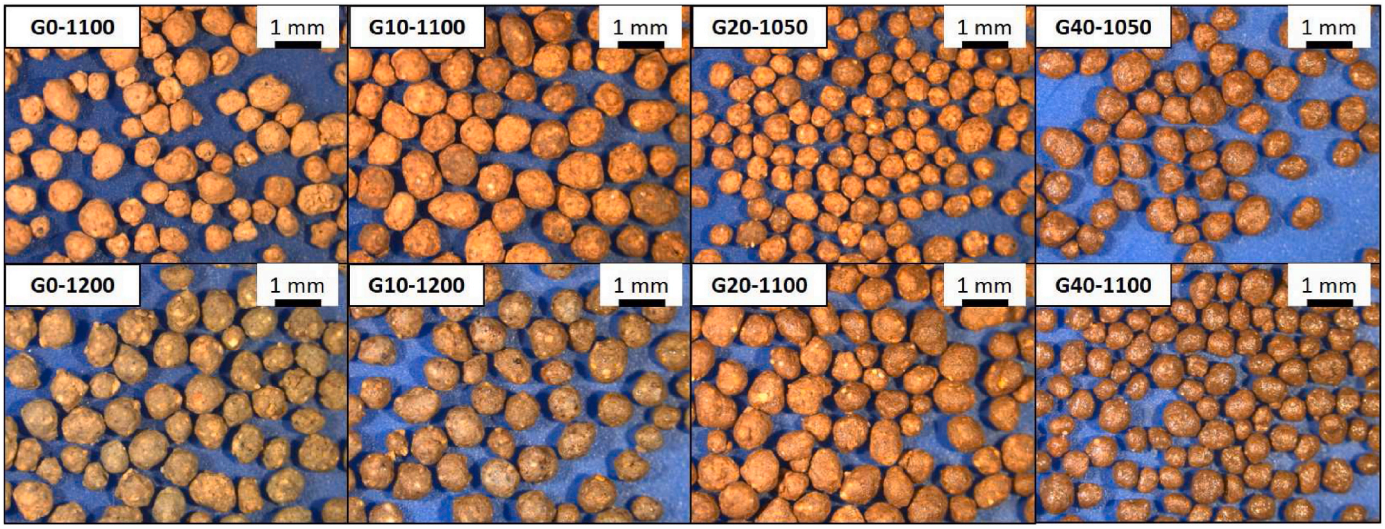

Fig. 4. Stereoscopic microscope images of the studied proppants.

Table 4
Apparent density, bulk density and breakage ratio values of the different samples.

Sample	G0		G10		G20		G40	
Firing temperature (°C)	1100	1200	1100	1200	1050	1100	1050	1100
Apparent density[a] (g/cm^3)	2.60	2.55	2.54	2.46	2.55	2.50	2.49	2.43
Bulk density[a] (g/cm^3)	1.26	1.34	1.32	1.32	1.36	1.37	1.36	1.38
Breakage ratio (wt.%)[a]	13.1	11.9	10.0	17.2	11.6	7.8	8.5	10.8
Acid solubility (wt.%)	8	6	11	6	12	12	12	12

[a] The standard deviation of the values is 0.01 for apparent density, 0.02 for bulk density and 0.1 for breakage ratio.

3.3. Characterization of proppants as a ceramic material

XRD patterns of samples fired at different temperatures are shown in Fig. 5. The crystalline phases associated with silica (SiO_2) in all the resulting proppants is quartz, and in most samples cristobalite is also identified. In G0 and G10 at booth temperatures and in G20-1100 samples mullite ($3Al_2O_3.2SiO_2$) was identified, and in G20 and G40 plagioclase ((Na,Ca) $(Si,Al)_3O_8$) is observed. In addition, peaks related to hematite (Fe_2O_3) are observed in all the proppants. By increasing the proportion of green glass in the starting mixture, the intensity of the cristobalite and hematite peaks increases. This is because green glass contributes significant amounts of SiO_2 and Fe_2O_3 to the mixture.

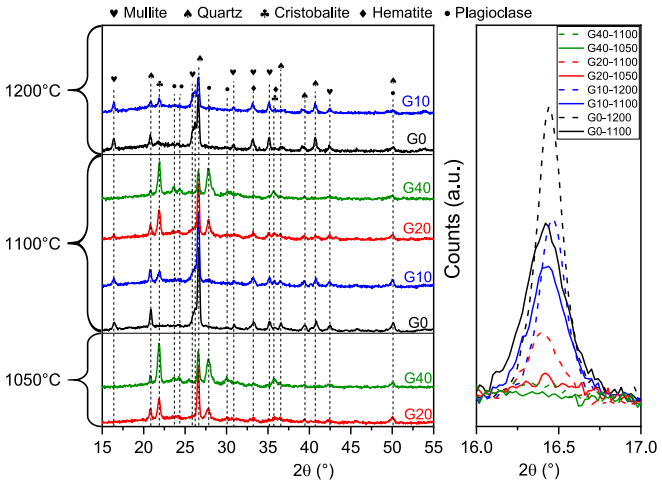

Fig. 5. XRD patterns of the samples after firing; the right plot is a zoom of the mullite peak (hkl 110). Peaks were identified using reference data (quartz (Q) PDF 01-089-1961; cristobalite (C) PDF 01-082-0512; hematite (H) PDF 01-07-0603; mullite (M) PDF 01-083-1565; plagioclase (P) PDF: 01-076-0898).

In the right plot of Fig. 5, the mullite 110 peak is shown with more detail. As was described in DTA curves (Fig. 1) the exothermic peak at 938 °C was not observed for G40 formulation and this is related to the absence of mullite in G40 samples.

SEM images of the surface of the fired proppants are shown in Fig. 6. In all images, a rough topography is observed, with few open pores and a predominant vitreous phase. Furthermore, as the amount of green glass in the formulation and the firing temperature increases, the roughness decreases due to a higher amount of vitreous phase. This is consistent with the decrease in apparent density observed in Table 4. As the surface permeability decreases, liquids cannot fill the internal pores and the apparent density of the granules decreases. In sample G0 it is observed how the increase in firing temperature favours the formation of a vitreous phase in the material, which also increases the densification of the material. In the rest of the samples, no significant microstructural variations with the firing temperature are observed.

Fig. 7 presents SEM micrographs for proppants G20 and G40 after the acid treatment. These images allow analysing the crystalline phases without vitreous phase. As can be observed, for the G20 fired at 1100 °C interlocked mullite needle-like grains are clearly present, with sizes up to about 5 μm. This sample presented the best performance in the crush test (lowest breakage ratio), which may be related to the observed microstructure [46]. This interlocked mullite needle-like microstructure was not observed in the other studied samples, even for the same formulation fired at 1050 °C. Fig. 7 also presents the case of the G40 proppant. In G40-1050 it can be observed crystals with irregular size and shape that could be associated with quartz and cristobalite phase (as obtained from the XRD patterns of Fig. 5), and in G40-1100 less of these grains are observed. According to the breakage ratio values of Table 4, G40-1050 is the second sample with best performance in the crush test, so in this case the mechanical resistance may be related to this

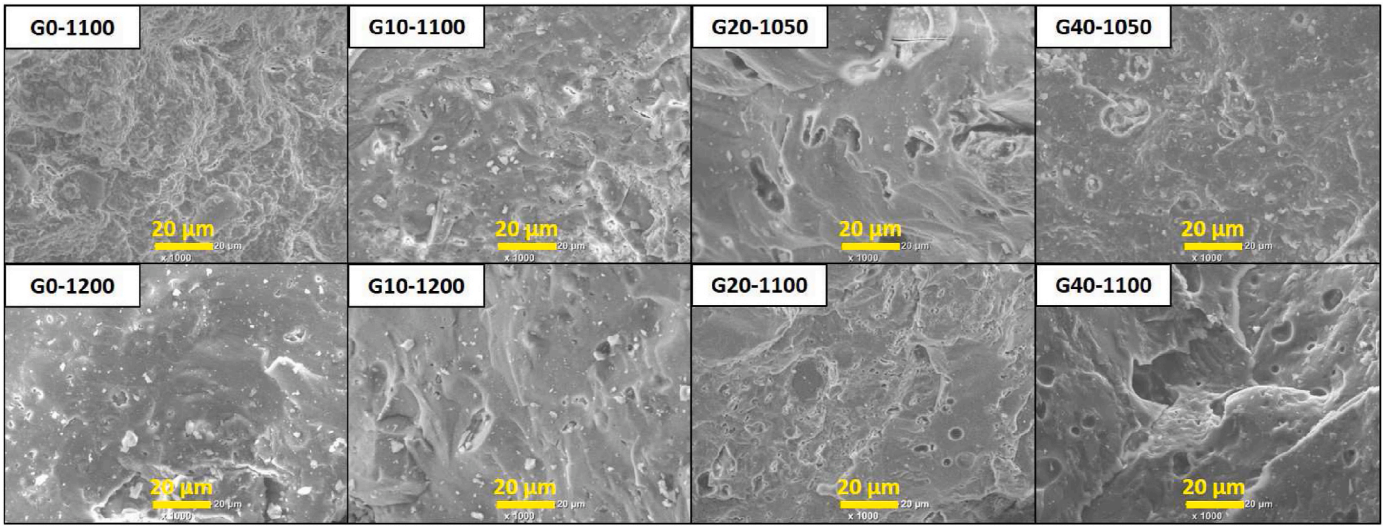

Fig. 6. SEM surface images of the different samples.

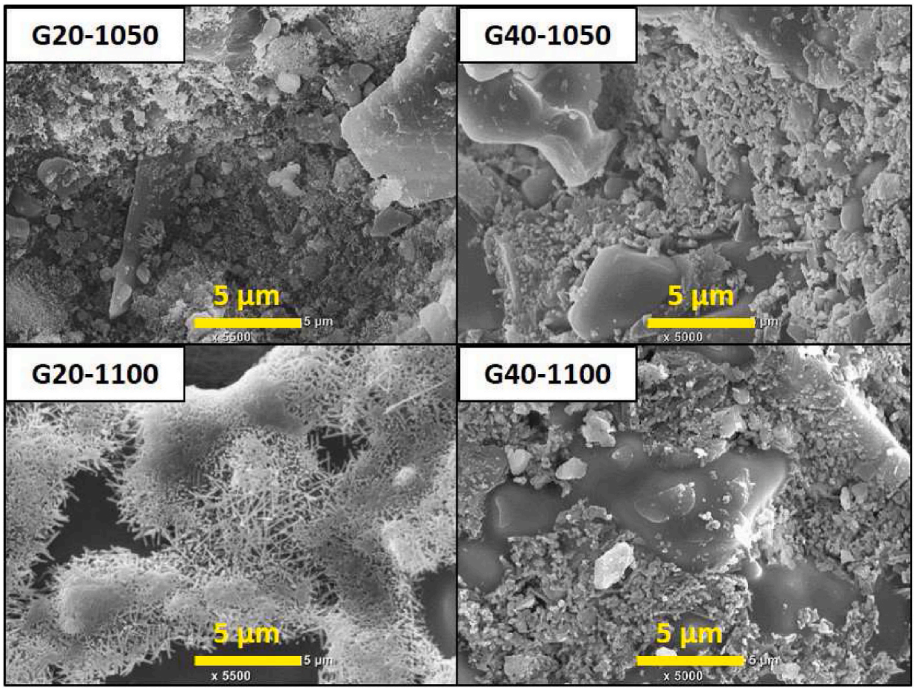

Fig. 7. SEM images after acid treatment of G20 and G40 samples.

microstructure.

A representative stress–strain curves for each material are shown in Fig. 8. The main characteristics observed in all these curves are the small initial curved area, followed by a linear behaviour until culminating in an abrupt drop in stress due to the fracture of the material. This behaviour is typical of a brittle fracture and is also commonly observed in the diametral compression stress curves of commercial proppants [30, 47–49].

In Table 5 are presented the average values for the diameter, the maximum load L and the tensile strength σ_T obtained for samples of the different proppants. It can be seen that the stress supported by the granules of the different samples ranges between 80 and 140 MPa. G20-1100 and G40-1050 have greater resistance than the other proppants, which is consistent with the results obtained in the crush tests (see Table 4). According to the obtained standard deviations, the maximum load and strength results present a dispersion of about 25 %, which is similar to those obtained for the authors in previous works [48,49]. These deviation values are within the expected range for ceramic materials that do not have a geometry as defined as that generally used in mechanical testing. Furthermore, the mechanical strength of a ceramic material generally depends on the volume of the material tested and the type of load configuration [50]. For this reason, the dispersion of the values obtained is significant. Therefore, this technique can be considered a very suitable alternative for performing a characterization of the proppants mechanical resistance, because it allows knowing their mechanical strength in shorter operating times and using lower quantities of material than crush test requires (10–20 granules in comparison to approximately 200 g).

4. Conclusions

It was possible to granulate proppants of appropriate size and shape

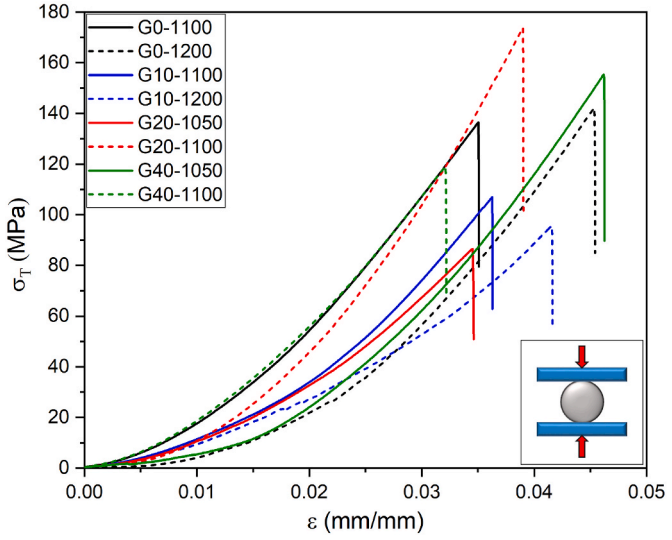

Fig. 8. Representative single grain diametral compression stress-strain curves of the studied materials (the scheme in the inset shows how this test is performed).

Table 5
Individual diametral compression values of the samples. Standard deviation is between brackets.

Sample	Diameter average (mm)	Max. Load average (N)	Stress average (MPa)
G0-1100	0.735	33 (11)	82 (27)
G0-1200	0.709	48 (12)	121 (30)
G10-1100	0.672	30 (12)	83 (32)
G10-1200	0.700	44 (13)	117 (34)
G20-1050	0.671	24 (6)	83 (16)
G20-1100	0.670	51 (23)	138 (62)
G40-1050	0.678	49 (7)	136 (21)
G40-1100	0.761	54 (16)	117 (36)

using the proposed formulations, which include traditional raw materials and reused bottle glass. Furthermore, through the present strategy for incorporating bottle glass, it was possible to lower the sintering temperature, which contributes to saving energy and costs in the firing stage. As a consequence, low-density proppants were obtained from economical raw materials, which includes significant quantities of an urban waste, and using a simple and low-cost processing route. The use of low-density proppants in hydrocarbon wells has the advantages of reducing the weight of proppant per well and, in addition, reducing the use of additives that control sedimentation in fracturing fluids, reducing total costs.

The obtained proppants from different starting formulations present similar performance or superior to that of some high-quality sands (crush test), with the advantage of having better sphericity and roundness, which could mean better conductivity of the hydrocarbons in the well. The only drawback identified in the proposed formulation is the acid solubility performance compared to products made only with clays and feldspars. However, in many specific well conditions this requirement is not critical and products with similar behaviour such as the one achieved would fully comply with the necessary request. Particularly, it could be concluded that the sample with the best performance was that involves 20 wt% of green glass and a sintering temperature of 1100 °C (sample G20-1100). This sample presented the best crush test performance, which can be related to its microstructure made of interlocked mullite needle-like grains and quartz crystals, all embedded in a vitreous phase.

CRediT authorship contribution statement

Ricardo Anaya: Writing – review & editing, Writing – original draft, Resources, Methodology, Investigation, Formal analysis, Data curation, Conceptualization. **María F. Hernández:** Writing – review & editing, Visualization, Conceptualization. **Anabella Mocciaro:** Writing – review & editing, Writing – original draft, Visualization, Conceptualization. **Diego Richard:** Writing – review & editing, Visualization, Conceptualization. **Nicolás M. Rendtorff:** Writing – review & editing, Supervision, Resources, Methodology, Funding acquisition, Conceptualization.

Declaration of competing interest

The authors declare that they have no known competing financial interests or personal relationships that could have appeared to influence the work reported in this paper.

Acknowledgments

This work has been supported by the Argentinian funding institutions Consejo Nacional de Investigaciones Científicas y Técnicas (CONICET), Agencia Nacional de Promoción Científica y Tecnológica (ANPCyT, PICT 2021–392 and 2021–774), and Facultad de Ciencias Exactas, Universidad Nacional de La Plata, UNLP, X-904). R.A. thanks CONICET for the posdoc scholarchip; M.F.H, A.M., D.R., and N.M.R. are members of CONICET, Argentina.

References

[1] Z. Liao, X. Li, L. Ge, Z. Yang, J. Zhu, Q. Xue, H. Wang, Lightweight proppants in unconventional oil and natural gas development: a review, Sustainable Materials and Technologies 33 (2022) e00484, https://doi.org/10.1016/j.susmat.2022.e00484.
[2] Q. Ren, Y. Ren, H. Li, X. Wu, W. Bai, J. Zheng, O. Hai, Preparation and characterization of high silicon ceramic proppants using low grade bauxite and fly ash, Mater. Chem. Phys. 230 (2019) 355–361, https://doi.org/10.1016/j.matchemphys.2019.04.009.
[3] T. Palisch, R. Duenckel, B. Wilson, New technology yields ultrahigh-strength proppant, SPE Prod. Oper. 30 (2015) 76–81, https://doi.org/10.2118/168631-PA.
[4] M. Abd El-Kader, M. Abdou, A. Fadl, A. Abd Rabou, O. Desouky, y M. El-Shahat, Novel light-weight glass-ceramic proppants based on frits for hydraulic fracturing process, Ceram. Int. 46 (2020) 1947–1953, https://doi.org/10.1016/j.ceramint.2019.09.173.
[5] M. Dondi, M. Raimondo, C. Zanelli, Clays and bodies for ceramic tiles: reappraisal and technological classification, Appl. Clay Sci. 96 (2014) 91–109, https://doi.org/10.1016/j.clay.2014.01.013.
[6] T. Wu, B. Wu, S. Zhao, Acid resistance of silicon-free ceramic proppant, Mater. Lett. 92 (2013) 210–212, https://doi.org/10.1016/j.matlet.2012.10.124.
[7] A. Mocciaro, M.B. Lombardi, A.N. Scian, Effect of raw material milling on ceramic proppants properties, Appl. Clay Sci. 153 (2018) 90–94, https://doi.org/10.1016/j.clay.2017.12.009.
[8] C. Zanelli, S. Conte, C. Molinari, R. Soldati, M. Dondi, Waste recycling in ceramic tiles: a technological outlook, Resour. Conserv. Recycl. 168 (2021) 105289, https://doi.org/10.1016/j.resconrec.2020.105289.
[9] L. Wietschel, F. Halter, A. Thorenz, D. Schüppel, D. Koch, Literature review on the state of the art of the circular economy of Ceramic Matrix Composites, Open Ceramics 14 (2023) 100357, https://doi.org/10.1016/j.oceram.2023.100357.
[10] X. Zou, The low temperature preparation of ultra low-density ceramic proppants by adding fly ash, Ceramics (2019) 107–114, https://doi.org/10.13168/cs.2019.0055.
[11] Y. Xiang, L. Han, Z. Xu, D. Hu, L. Ning, Y. Yu, S. Gao, C. Li, J. Xu, Preparation of drilling cuttings-coal fly ash based ceramic proppants: the roles of barite, Ceram. Int. 49 (2023) 25530–25542, https://doi.org/10.1016/j.ceramint.2023.05.093.
[12] N. Toniolo, A.R. Romero, M. Marangoni, M. Binhussain, A.R. Boccaccini, y E. Bernardo, Glass-ceramic proppants from sinter-crystallisation of waste-derived glasses, Adv. Appl. Ceram. 117 (2018) 127–132, https://doi.org/10.1080/17436753.2017.1394019.
[13] M. Dondi, Feldspathic fluxes for ceramics: sources, production trends and technological value, Resour. Conserv. Recycl. 133 (2018) 191–205, https://doi.org/10.1016/j.resconrec.2018.02.027.

[14] R. Rawlings, J. Wu, A. Boccaccini, Glass-ceramics: their production from wastes—a review, J. Mater. Sci. 41 (2006) 733–761, https://doi.org/10.1007/s10853-006-6554-3.
[15] E. Bernardo, E. Bonomo, A. Dattoli, Optimisation of sintered glass–ceramics from an industrial waste glass, Ceram. Int. 36 (2010) 1675–1680, https://doi.org/10.1016/j.ceramint.2010.02.047.
[16] R.K. Chinnam, A.A. Francis, J. Will, E. Bernardo, A.R. Boccaccini, Review. Functional glasses and glass-ceramics derived from iron rich waste and combination of industrial residues, J. Non-Cryst. Solids 365 (2013) 63–74, https://doi.org/10.1016/j.jnoncrysol.2012.12.006.
[17] M. Dondi, G. Guarini, M. Raimondo, C. Zanelli, Recycling PC and TV waste glass in clay bricks and roof tiles, Waste Manag. 29 (2009) 1945–1951, https://doi.org/10.1016/j.wasman.2008.12.003, jun. 2009.
[18] M.F. Hernández, M.S. Conconi, M. Cipollone, M.S. Herrera, y N.M. Rendtorff, Ceramic behavior of ball clay with gadolinium oxide (Gd_2O_3) addition, Appl. Clay Sci. 146 (2017) 380–387, https://doi.org/10.1016/j.clay.2017.06.021.
[19] C. Zanelli, Raimondo, M.R. Raimondo, G. Guarini, M. Dondi, C. Iglesias, E. Dominguez, R. Ullmann, Improving technological performances of ball clays: a case-study from patagonia (Argentina), Accesed 29 March 2024, http://hdl.handle.net/11336/73203, 2011.
[20] V. Savić, V. Topalović, J. Nikolić, S. Jevtić, N. Manić, M. Komatina, S. Matijašević, S. Grujić, Foam glasses made from green bottle glass and sugar beet factory lime as a foaming agent, Heliyon 9 (2023) e17664, https://doi.org/10.1016/j.heliyon.2023.e17664.
[21] V. Vaitkevičius, E. Šerelis, D. Vaičiukynienė, V. Raudonis, Ž. Rudžionis, Advanced mechanical properties and frost damage resistance of ultra-high performance fibre reinforced concrete, Construct. Build. Mater. 126 (2016) 26–31, https://doi.org/10.1016/j.conbuildmat.2016.09.012.
[22] K. Ax, H. Feise, R. Sochon, M. Hounslow, A. Salman, Influence of liquid binder dispersion on agglomeration in an intensive mixer, Powder Technol. 179 (2008) 190–194, https://doi.org/10.1016/j.powtec.2007.06.010.
[23] E. Schaer, C. Gagnard, L. Choplin, D. Canpont, Experimental tracking of silica dispersion into silicone polymer, Powder Technol. 168 (2006) 156–166, https://doi.org/10.1016/j.powtec.2006.06.006.
[24] M.S. Conconi, M. Morosi, J. Maggi, P.E. Zalba, F. Cravero, y N.M. Rendtorff, Thermal behavior (TG-DTA-TMA), sintering and properties of a kaolinitic clay from Buenos Aires Province, Argentina, Cerâmica 65 (2019) 227–235, https://doi.org/10.1590/0366-69132019653742621.
[25] J.M. Martinez, M.S. Conconi, F. Booth, y N.M. Rendtorff, High-temperature transformations of Zr-pillared bentonite, J. Therm. Anal. Calorim. 145 (2021) 51–58, https://doi.org/10.1007/s10973-020-09681-0.
[26] R.P.19C. Api, Measurement of Properties of Proppants Used in Hydraulic Fracturing and Gravel-Packing Operations, American Petroleum Institute, 2020-09. ISO 13503-2:2006 identical.
[27] A. Kamel, Z. Salem, R. Chemini, M. Khodja, y K. Allia, Characterization of natural sand proppant used in hydraulic fracturing fluids, Part. Sci. Technol. 37 (2019) 716–724, https://doi.org/10.1080/02726351.2018.1438542.
[28] W. Zheng, S.C. Silva, y D.D. Tannant, Crushing characteristics of four different proppants and implications for fracture conductivity, J. Nat. Gas Sci. Eng. 53 (2018) 125–138, https://doi.org/10.1016/j.jngse.2018.02.028.
[29] M.S. Conconi, M.R. Gauna, M.F. Serra, G. Suarez, E.F. Aglietti, y N.M. Rendtorff, Quantitative firing transformations of a triaxial ceramic by X-ray diffraction methods, Cerâmica 60 (2014) 524–531, https://doi.org/10.1590/S0366-69132014000400010.
[30] R. Anaya, J.M. Martínez, M.F. Hernández, M.S. Herrea, y N.M. Rendtorff, Individual diametral compression behavior of a ceramic proppant, Ceram. Int. 48 (2022) 32357–32365, https://doi.org/10.1016/j.ceramint.2022.07.179.
[31] Y. Hiramatsu, Y. Oka, Determination of the tensile strength of rock by a compression test of an irregular test piece, Int. J. Rock Mech. Min. Sci. Geomech. Abstracts 3 (1966) 89–90, https://doi.org/10.1016/0148-9062(66)90002-7.
[32] L. Andrini, M.R. Gauna, M.S. Conconi, G. Suarez, F.G. Requejo, E.F. Aglietti, N. M. Rendtorff, Extended and local structural description of a kaolinitic clay, its fired ceramics and intermediates: an XRD and XANES analysis, Appl. Clay Sci. 124–125 (2016) 39–45, https://doi.org/10.1016/j.clay.2016.01.049.
[33] W.E. Lee, G.P. Souza, C.J. McConville, T. Tarvornpanich, Y. Iqbal, Mullite formation in clays and clay-derived vitreous ceramics, J. Eur. Ceram. Soc. 28 (2008) 465–471, https://doi.org/10.1016/j.jeurceramsoc.2007.03.009.
[34] H. Schneider, B. Saruhan, D. Voll, L. Merwin, A. Sebald, Mullite precursor phases, J. Eur. Ceram. Soc. 11 (1993) 87–94, https://doi.org/10.1016/0955-2219(93)90062-V.
[35] L. Carbajal, F. Rubio-Marcos, M.A. Bengochea, y J.F. Fernandez, Properties related phase evolution in porcelain ceramics, J. Eur. Ceram. Soc. 27 (2007) 4065–4069, https://doi.org/10.1016/j.jeurceramsoc.2007.02.096.
[36] A.K. Chakraborty, D.K. Ghosh, Reexamination of the kaolinite-to-mullite reaction series, J. Am. Ceram. Soc. 61 (1978) 170–173, https://doi.org/10.1111/j.1151-2916.1978.tb09264.x.
[37] H. Schneider, J. Schreuer, y B. Hildmann, Structure and properties of mullite—a review, J. Eur. Ceram. Soc. 28 (2008) 329–344, https://doi.org/10.1016/j.jeurceramsoc.2007.03.017.
[38] M.F. Hernández, P.V. López, M.S. Conconi, y N.M. Rendtorff, Effect of boron sources in the thermal behavior of a clay-based ceramics, Open Ceramics 9 (2022) 100227, https://doi.org/10.1016/j.oceram.2022.100227.
[39] L.V. Lehman, M.A. Parker, M.E. Blauch, R. Haynes, A. Blackmon, Proppant Conductivity — what Counts and Why, Society of Petroleum Engineers, 1999 52219, https://doi.org/10.2118/52219-MS.
[40] J. Xu, Y. Ding, L. Yang, Z. Liu, R. Gao, H. Yang, Z. Wang, Conductivity analysis of tortuous fractures filled with non-spherical proppants, J. Petrol. Sci. Eng. 198 (2021) 108235, https://doi.org/10.1016/j.petrol.2020.108235.
[41] A.S. Ramlan, R.M. Zin, N.F.A. Bakar, N.H. Othman, Recent progress on proppant laboratory testing method: characterisation, conductivity, transportation, and erosivity, J. Petrol. Sci. Eng. 205 (2021) 108871, https://doi.org/10.1016/j.petrol.2021.108871.
[42] X. Wu, Z. Huo, Q. Ren, H. Li, F. Lin, y T. Wei, Preparation and characterization of ceramic proppants with low density and high strength using fly ash, J. Alloys Compd. 702 (2017) 442–448, https://doi.org/10.1016/j.jallcom.2017.01.262.
[43] B. Zboromirska-Wnukiewicz, K. Kasprzyk, K. Kogut, y A. Dyjakon, Preparation of a ceramic proppants for hydraulic fracturing using F – type fly ash, Arch. Metall. Mater. 63 (2018) 1065–1070, https://doi.org/10.24425/122444.
[44] G. Wahab, G. Ibrahim, A. Wahab, Geological and engineering appraisal of hydraulic frac sand in some Egyptian localities as a proppant of oil well drilling, Heliyon 8 (2022) e10233, https://doi.org/10.1016/j.heliyon.2022.e10233.
[45] N. John, I. Khan, A. Patel, Evaluation of the crushing characteristics of industrial waste aggregates as construction materials, Construct. Build. Mater. 403 (2023) 133111, https://doi.org/10.1016/j.conbuildmat.2023.133111.
[46] P.V. López, M.F. Hernández, D. Richard, M.S. Conconi, N.M. Rendtorff, Porous acicular mullite ceramics produced from well and poorly crystallized kaolinite, Appl. Clay Sci. 238 (2023) 106937.
[47] N. Müller, V. Kilikoglou, P. Day, G. Vekinis, Thermal shock resistance of tempered archaeological ceramics, Craft and science: International perspectives on archaeological ceramics (2014) 263–270, https://doi.org/10.5339/uclq.2014.cas.ch28.
[48] I.D. Marinescu, M. Pruteanu, Chapter 2 - deformation and fracture of ceramic materials, in: Handbook of Ceramics Grinding and Polishing, second ed., 2015, pp. 50–66, https://doi.org/10.1016/B978-1-4557-7858-4.00002-9.
[49] T.B. Aulia, Rinaldi, bending capacity analysis of high-strength reinforced concrete beams using environmentally friendly synthetic fiber composites, Procedia Eng. 125 (2015) 1121–1128, https://doi.org/10.1016/j.proeng.2015.11.136.
[50] A.S. Jayatilaka, Fracture of engineering brittle materials, Applied Science Publishers (1979) 116–123. ISBN 0 85334 825 1.